Dependence of the scatter of the electrical properties on local non-uniformities of the tunnel barrier in Nb/Al-AlO$_x$/Nb junctions

Parisa Yadranjee Aghdam, Hawal Marouf Rashid, Alexey Pavolotsky, Vincent Desmaris, and Victor Belitsky
Department of Earth and Space Sciences, Chalmers University of Technology, Gothenburg 41296, Sweden

In this paper, we study the effect of the tunnel barrier thickness non-uniformity in Nb/Al-AlO$_x$/Nb tunnel junctions using the measurement results of the junction capacitance (C) and the normal resistance (R_n). The local thickness distribution of the AlO$_x$ tunnel barrier in Nb/Al-AlO$_x$/Nb trilayer ($R_nA \sim 30$ Ω μm^2) was studied by high resolution transmission electron microscopy. The specific resistance (R_nA) values of the measured junctions range from 8.8 to 68 Ω μm^2. We observed scatter in both the junction specific resistance and capacitance data, which is considerably higher than the measurement uncertainty. We also observed noticeable scatter in the R_nC product, which does not stem from junction area estimation uncertainties. We discuss the possible reasons that contribute to this scatter. We suggest that the local thickness non-uniformity of the tunnel barrier significantly contributes to the scatter in the R_nC product. We confirm this conclusion through an illustrative model based on the barrier imaging data, which results in the variation of the R_nC data consistent with the measurements in this paper. © 2016 AIP Publishing LLC.
[http://dx.doi.org/10.1063/1.4941346]

I. INTRODUCTION

Superconductor-Insulator-Superconductor (SIS) Nb/Al-AlO$_x$/Nb tunnel junctions are widely used in superconducting electronic devices such as SIS mixers, SQUIDs, qubits, single charge, and digital circuits.[1] In these devices, at high transparency of the tunnel barrier, the control of the junction parameters such as current density (J_c), the specific resistance (R_nA = normal resistance × area), and the specific capacitance (C_s = junction capacitance (C)/Area) becomes challenging due to the scatter of these parameters for junctions on the same wafer.

Previous studies have often suggested that the scatter of J_c and R_nA is due to the junction size variations.[2–5] It should be noted that, for the high quality junctions, the observed scatter probably cannot completely be attributed to the variation of the junction area. The existence of pinholes, defects, and local thickness non-uniformities in the tunnel barrier creates quantum channels with very high transparencies, which can lead to higher order tunneling processes[6–11] and result in scatter in J_c and R_nA values. However, if the distribution of defects is uniform,[12–14] then the local scatter in R_n and J_c values will average out over the junction size, and hence, R_n and J_c values would not change over the wafer area. If the defects are not uniformly dispersed over the wafer area, the junctions' R_n and J_c values would experience scatter.[15,16] This is the case for high quality junctions, which have less non-uniformities per junction area. Therefore, averaging out the effect of these non-uniformities is less probable at the junction size scale.

In this paper, we report that a considerable scatter is observed in the measured R_nA and C_s data of Nb/Al-AlO$_x$/Nb SIS junctions. The junction capacitance is measured directly and accurately using the previously demonstrated method.[17] We characterized junctions with nominal sizes 3.6–20 μm^2 and R_nA values ranging from 8.8 to 68 Ω μm^2, which correspond to $J_c \sim 3$–26 kA/cm^2. Since it is suspected that the junction area estimation can considerably contribute to the scatter in R_nA and C_s, the R_nC product, which is junction area independent, is used to identify the origin of the scatter. The scatter in the R_nC product of the junctions in each wafer is almost constant over the investigated R_nA range. The observed scatter was considerably higher than the measurement uncertainty, which rules out the scatter due to the measurement error. We interpret this fact such that the scatter in the measured data should be mainly attributed to the difference in the local distribution of the barrier thickness over the junction area.

In addition to the electrical characterization of the junctions, the microstructure of the AlO$_x$ tunnel barrier in Nb/Al-AlO$_x$/Nb trilayer with $R_nA \sim 30$ Ω μm^2 is investigated with the use of the high resolution transmission electron microscopy (HRTEM). It is found that the AlO$_x$ tunnel barrier thickness is non-uniform and varies between 0.9 nm to 1.6 nm over a $\sim$35 nm wide HRTEM cross-section image. Using an illustrative model and taking into account the obtained thickness distribution, we show that the R_nC scatter can originate from local variations in the thickness distribution of the tunnel barrier.

II. EXPERIMENT

A. Sample preparation

The Nb/Al-AlO$_x$/Nb junctions were fabricated on 30 × 30 mm^2 high resistivity Si substrates. The trilayer deposition parameters and the junction fabrication follow the process described in Refs. 17 and 18. Each wafer contained seven chips. Six batches (each batch contained one or two

wafers) with different R_nA values were fabricated. The tunnel barrier was formed by exposing the fresh Al surface to oxygen. The oxygen exposure (E), the product of the oxygen pressure P_{ox} and time, is used as an indicator of the oxidation strength. The different batches of junctions were subjected to different oxygen exposures. Table I summarizes the oxidation parameters and the number of the measured samples for the batches of the junctions presented in the paper.

Each chip contained an SIS junction connecting the superconducting Nb 50 Ω microstripline (6 mm long, 550 μm wide) and the ground plane. The chip is mounted into a fixture (copper piece), which connects the junction to the SMA (Subminiature A) connector with sliding pin. The junctions have the nominal areas: $A1 = 3.6\ \mu\text{m}^2$, $A2 = 4.4\ \mu\text{m}^2$, $A3 = 6\ \mu\text{m}^2$, $A4 = 10.8\ \mu\text{m}^2$, and $A5 = 20\ \mu\text{m}^2$. A total of 34 Nb/Al-AlO$_x$/Nb tunnel junctions were characterized, which have different barrier thicknesses with R_nA ranging between 8.8 and 68 $\Omega\ \mu\text{m}^2$. The junction size (A_e) is extracted following the procedure in Ref. 17, taking into account the dimension variation due to the fabrication process (lithography and etch process). On each wafer, contact pads were fabricated allowing dc IV characteristic recording at 4.2 K. The junction characteristic parameters, normal resistance (R_n), subgap resistance (R_{sg}), and superconducting gap voltage (V_g), were extracted from the recorded IV characteristic of the junctions measured in liquid helium.[19] In this study, the R_n value is estimated as the average resistance measured when biasing the junction with voltages between 5.5 mV and 6 mV. The R_{sg} is defined as the slope of the line going through the coordinate origin (0,0) and the IV characteristic at 2 mV. In this paper, instead of the critical current density, we use the R_nA_e (henceforth denoted as R_nA) value as the measure of the tunnel barrier transparency. The fabricated junctions demonstrate excellent quality characterized by the following parameters in a wafer: $V_g \simeq 2.84\ldots2.88$ mV, $R_nA \simeq 8.8\ldots68$ $\Omega\ \mu\text{m}^2$, and $R_{sg}/R_n \simeq 17\ldots44$. A typical IV characteristic is presented in Fig. 1.

The junction capacitance measurement method[17] relied on recording of the complex reflection coefficient, S_{11}, at the frequency 4 GHz when the junction is biased at the subgap voltage (1 mV). Since the measurements are performed at cryogenic temperatures and the induced temperature gradient alters cable characteristics, a dedicated calibration procedure[17,20] was applied in these measurements.

B. HRTEM analysis

In this paper, the cross-section HRTEM analysis of the tunnel barrier in Nb/Al-AlO$_x$/Nb trilayer was performed. The specimens were prepared by gluing the two pieces of the

TABLE I. Oxygen exposure (E) for the six different batches fabricated in this study. The number of chips characterized is also indicated.

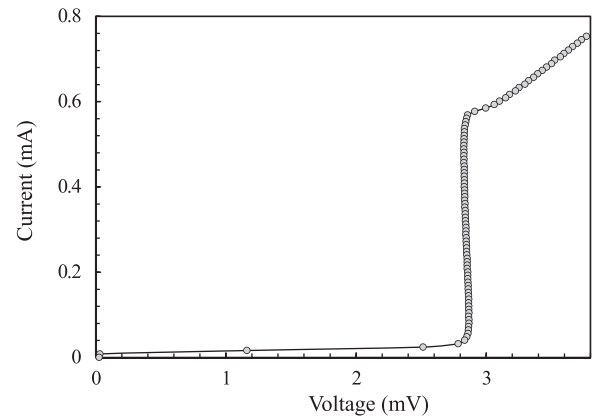| Batch number	1	2	3	4	5	6
E (Pa s)	1530	1530	2500	2500	6200	13000
Wafers	1	2	1	1	2	2
Chips	3	5	5	5	8	8

FIG. 1. The IV characteristic of a junction with nominal area of $A2 = 4.4\ \mu\text{m}^2$ and estimated R_nA value of $\simeq 8.8\ \Omega\ \mu\text{m}^2$. The junction quality factor is $R_{sg}/R_n \simeq 17.5$. The slight back bending as a result of overheating effects can be seen.

sample face to face. The stack was diced into $\sim$300 μm thick pieces. The cross-sections were polished into a wedge shape perpendicular to the layers. At the final stage, the sample was thinned to electron transparency by Ar ion milling (Precision Ion Polishing System, PIPS, Gatan, Inc.). The TEM investigations were performed at 300 kV using a FEI Titan 60–300 TEM equipped with the spherical aberration image-corrector.

III. RESULTS AND DISCUSSION

A. Evaluation of the C_s and R_nA data

In the performed measurements, special care was taken to ensure that the measured capacitance is the true geometrical capacitance, and hence, any other possible contribution, e.g., stray capacitance, should be excluded. As it was discussed in another study,[21] the stray capacitance could be a result of a parallel circumferential capacitance due to the high dielectric constant ($\varepsilon_r \sim 30$) of Nb$_2$O$_5$ as a result of the anodization in the junction fabrication process. The thickness of Nb$_2$O$_5$ is reported to be in the range of 0.85–2 nm per voltage (V) of the anodization voltage.[21–23] Therefore, considering the anodization rate of 2 nm/V and the anodization voltage of 13 V, the anodized thickness of Nb$_2$O$_5$ would be $\sim$26 nm. With the top electrode of 100 nm thick and assuming a parallel-plate approximation, this parasitic capacitance was found to be insignificant for the smallest and the largest junctions, 0.5 fF and 1.1 fF, respectively. In addition, the contribution from the fringing-field capacitance using the 2D Palmer formula[24] was calculated and as well was negligible. However, the contribution to the measured junction capacitance resulting from the non-linearity of the quasiparticle current-voltage characteristic as follows from the Kramers-Kronig transform[25] was found to be significant. This nonlinear capacitance was calculated for all the junctions using the model in Ref. 26. Henceforth, the presented results of the capacitance are the corrected junction capacitance (with subtracted contribution of nonlinear capacitance).

The true area of a junction can hardly be accurately measured, since the visible "printout" (see Fig. 2) of the junction is affected by the layers covering the junction
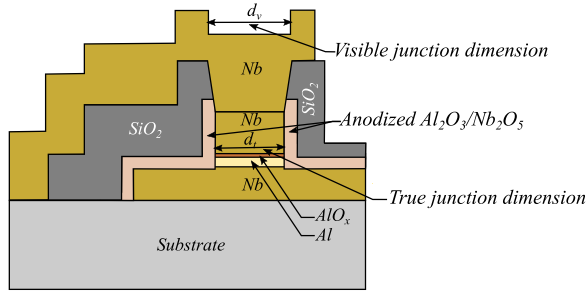
FIG. 2. Schematic cross-section of a typical SIS tunnel junction. The visible (d_v) and the true (d_t) dimensions of the junction are shown.

FIG. 4. $R_nC/(R_nC)_{avg}$ as a function of O_2 exposure for all the characterized junctions with areas ranging from $A1 = 3.6$ to μm^2 to $A5 = 20\,\mu m^2$.

stencil (SiO_2 dielectric and Nb line layers). Therefore, the junction area can only be estimated.[17] Using the measured R_n and C, and the estimated junction area, the junction specific resistance, R_nA, and the specific capacitance, C_s, are plotted in Figs. 3(a) and 3(b), respectively, as functions of the oxygen exposure. It is evident that both the R_nA and C_s data demonstrate a noticeable scatter. It is often considered that the observed scatter is due to the estimation of the junction area and nonuniform area variations across the wafer.[2–5] Alternatively, others[6–11] state that it is the non-uniformity of the tunnel barrier itself which is responsible for the scatter of the specific resistance and, as we suggest, the specific capacitance of tunnel junctions.

To distinguish between the extrinsic (area variations) and intrinsic (e.g., barrier thickness non-uniformities) origins of the scatter of the tunnel barrier parameters, we use the product of the specific resistance and the specific capacitance $R_nA \times C/A$, which is area independent. As shown in Fig. 4, the R_nC data normalized by the average R_nC of each batch experience scatter. In Fig. 4, the junction areas are also shown.

The observed scatter of as much as about 40% in the normalized R_nC in Fig. 4 points out that the origin of this scatter cannot be attributed to the area estimation. We however found that the measurement uncertainty of the R_nC varies depending on the junction area and is between just $\pm 2\%$ to $\pm 11.2\%$ for the largest and smallest junctions among all the batches, respectively.[27] Therefore, the scatter of the area-independent R_nC product emphasizes that the scatter also has intrinsic origins, e.g., the barrier thickness non-uniformity. In order to show this, the tunnel barrier thickness distribution needs to be found. In this study, we use direct imaging of the tunnel barrier by means of HRTEM
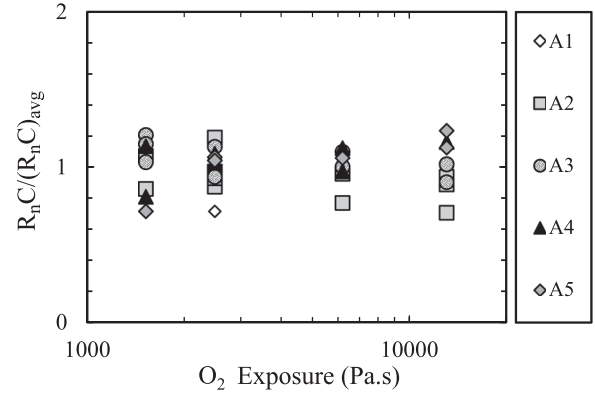
for extracting the data on the tunnel barrier thickness distribution. Knowing that, we can figure out if and which type of barrier thickness non-uniformities would result in the spread of the experimentally measured R_nC product.

Previously, continuously variable-thickness model[28] (uniform thickness increasing continuously) or the one-step model[29] (the junction area is divided into two portions with n and n + 1 monolayers) of the SIS junction tunnel barrier was suggested to illustrate the tunnel barrier thickness distribution. These models were used for fitting the relation between the measured specific capacitance and the specific resistance data. Using the continuously variable-thickness model,[28] it was attempted to extract the tunnel barrier height and the dielectric constant. However, in this approach, the barrier height shape was assumed to be rectangular with the same value for all the junctions with various transparencies. As a result, the obtained barrier height and the dielectric constant are often not physical. As for the one-step model, it was noted by the authors[29] that this approach becomes invalid at $J_c > 20\,kA/cm^2$, where according to Ref. 29, the tunnel barrier consists of only one monolayer thick oxide.

B. HRTEM analysis and the tunnel barrier model

The HRTEM analysis performed in our study, illustrated in Fig. 5(a), shows that the AlO_x layer is amorphous and the concept of monolayers is probably not applicable in the case of amorphous films.[28] Hence, the one-step[29] model of the tunnel barrier is not suitable. In this paper, the thickness of the AlO_x amorphous layer is extracted using the image intensity profile (see Fig. 5(b)). The blue boxes in Fig. 5(a) show
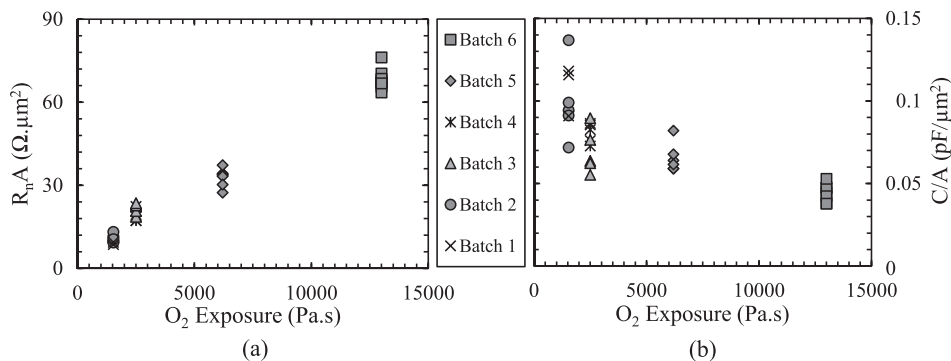

FIG. 3. Dependence of (a) the specific normal resistance (R_nA) and (b) the specific capacitance (C/A) on O_2 exposure. Different batches can be distinguished using the assigned marker as shown in the legend.
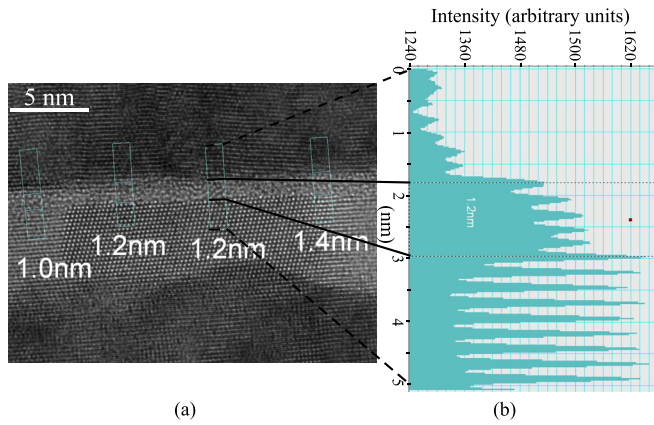
FIG. 5. (a) The HRTEM image of the Nb/Al-AlO$_x$/Nb SIS tunnel structure with expected $R_nA \sim 30$ Ω μm^2. The AlO$_x$ barrier thickness measurements are shown for each window. These measurements are obtained from intensity profiles (b) taken at each illustrated window in (a).

the sampling windows used for building the image intensity profiles. Inside the sampling window, the image intensity was averaged along its short side. The obtained intensity profile along the long side of the profile window was plotted (Fig. 5(b)). The image intensity profile has segments with different period and amplitude of the intensity oscillations corresponding to Al, AlO$_x$ tunnel barrier, and Nb layers. The thickness of the tunnel barrier in the given sampling window was read out as the distance between the endpoints of the segment corresponding to the AlO$_x$ tunnel barrier (presented as the distance between dashed lines in Fig. 5(b)). The results of this analysis show that the nonuniformity of the tunnel barrier thickness is not negligible and presenting it as a continuously variable-thickness[28] model is an oversimplification.

The tunnel barrier thickness distribution of the 35 nm wide cross-section image was extracted using 0.7 nm wide sampling windows and presented with black bars in Fig. 6. This distribution (black bars in Fig. 6) does not follow a Gaussian distribution unlike the results of the two recent studies,[30,31] which performed cross-section HRTEM analysis of thermally grown AlO$_x$ tunnel barrier. We believe that the reason for this dissimilarity is that the mentioned studies[30,31]
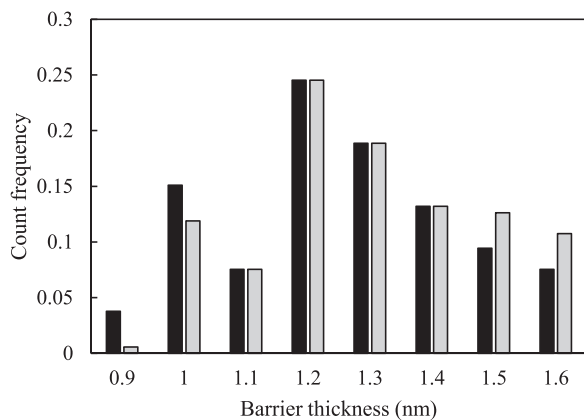

FIG. 6. AlO$_x$ barrier thickness distribution measured along a 35 nm wide HRTEM image (black bars) for Nb/Al-AlO$_x$/Nb structure with $R_nA \sim 30$ Ω μm^2. The suggested four bins variation is applied to the barrier thickness distribution as grey bars.

analyzed the thickness distribution of great number of points in their samples, and also, the type of junctions was different (Al/AlO$_x$/Al[30] and Cu/AlO$_x$/Al[31]) from our junctions. We suggest that, if the thickness distribution obtained from many more points over the wafer was used, the local thickness variations would be averaged out. Therefore, in order to investigate the effect of local thickness non-uniformities on R_nC value, we used the measured distribution (see Fig. 6), assuming that it is extended to the junction area.

In order to calculate the R_nC value, we employed a straightforward approach, which assigns a fraction of the total junction area ($A_{total} = 1$) to each barrier thickness of the distribution. The R_nA value is calculated using the tunneling theory,[32] assuming a uniform barrier thickness (d) for each area fraction

$$R_nA_f = \frac{h^2 d \, \exp\left(\frac{4\pi d\sqrt{2m\varphi}}{h}\right)}{e^2\sqrt{2m\varphi}}, \qquad (1)$$

where h is the Planck's constant, m is the effective electron mass, and e is the unit charge. The parallel connection of resistances of all the area fractions is considered as the R_n of the junction. Although the real Nb/Al-AlO$_x$/Nb junctions have an asymmetric barrier, for simplification reasons, a rectangular barrier height (φ) is assumed. Also, the free electron mass is used here. The reported data on the tunnel barrier height range from 0.1 up to 8.6 eV.[33–36] The barrier height with the value of $\sim$0.5 eV is used as a tuning parameter to set the range of the calculated R_nA around the expected value for the HRTEM sample and the batch 5, which employed identical Nb/Al-AlO$_x$/Nb trilayer structures.

The C is calculated using the parallel-plate approximation, assuming a dielectric constant of the tunnel barrier to be 9.5

$$C = \frac{A_f \varepsilon_0 \varepsilon_r}{d}. \qquad (2)$$

In order to show the scatter, variations in some of the area fractions (A_f) were suggested and thus are applied (see Fig. 6, compare grey bars with the measured black bars). Since the R_n and C are most sensitive to the thinnest and the thickest barrier, respectively, the variations were subjected to the corresponding area fractions. For instance, in Fig. 6 (grey bars), the area fraction of the two lowest thickness $d = 0.9$ nm and 1 nm was decreased by the same amount that was added to the area fraction of $d = 1.5$ nm and 1.6 nm to keep the total area unchanged. This variation in the thickness distribution results in scatter in both the R_nA and the R_nC. It should be mentioned that using a different value of the barrier height can result in a slightly different scatter. For instance, $\varphi = 0.5$ eV ± 0.1 eV ($\pm 20\%$) results in $\pm 8\%$ change of scatter in the R_nC product.

C. Comparison of the electrical characterization and the modelled data

In Fig. 7, the scatter range of the measured R_nC data (normalized to the $(R_nC)_{avg}$ of each batch) is illustrated with
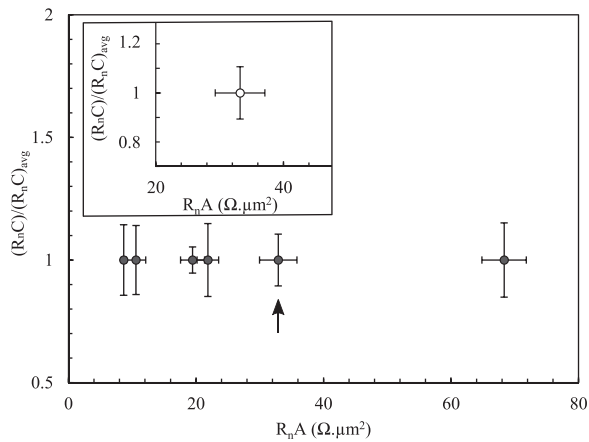
FIG. 7. The scatter of the measured normalized R_nC data as a function of R_nA is shown with standard deviation error bars. The inset depicts the scatter of the calculated R_nA and R_nC for the Nb/Al-AlO$_x$/Nb structure by applying four bin variation to its measured barrier thickness distribution (see Fig. 6). The exposure conditions for this sample are the same as batch 5, which is pointed by an arrow.

standard deviation error bars around the mean values (filled circles). The inset in Fig. 7 shows the scatter of the modelled R_nC data using the applied four bins variation as illustrated with grey bins in Fig. 6. The scatter in the modelled R_nC data can be compared to the measured R_nC of batch 5 pointed by an arrow in Fig. 7. This comparison shows that the calculated scatter in R_nC is as much as the scatter in the measured data. Therefore, using the measured tunnel barrier thickness distribution, the scatter in the R_nC product could be explained. However, the essential assumption was made that the locally measured thickness distribution is extended over the junction area. This assumption means that the spatial distribution of nanoscale regions with thickness much smaller than the mean thickness is considered to be quite narrow and non-uniform across the wafer. Therefore, the resulted self-averaging electrical properties of each junction could significantly vary across the wafer, leading to the scatter of both the R_nA and C_s. The above mentioned assumption is most likely the case for high quality junctions[2] rather than junctions, which contain higher number of the tunnel barrier defects. From the measured dc IV characteristics of the tested junctions (e.g., Fig. 1), it was inferred that our junctions are of high quality with $R_{sg}/R_n \geq 17$ for high current densities of $J_c \leq 26\,\text{kA/cm}^2$.

IV. CONCLUSION

In summary, we studied the scatter of the specific capacitance and the specific resistance data using the measured R_nC product, which removes uncertainties related to the junction area estimations. The capacitance of SIS tunnel junctions with various R_nA ranging from 8.8 to 68 Ω μm^2 was directly measured by employing a dedicated cryogenic calibration technique. We achieved very low measurement uncertainties down to $\pm 2\%$ for the measured R_nC product of junctions with large areas. The noticeable scatter observed in the R_nC data proves that tunnel barrier properties, e.g., the tunnel barrier thickness, are non-uniform across the wafer. The local thickness distribution of the AlO$_x$ tunnel barrier in

Nb/Al-AlO$_x$/Nb trilayer ($R_nA \sim 30$ Ω μm^2) was obtained using a high resolution transmission electron microscopy. Using an illustrative model, we demonstrated that the local variations in the thickness distribution of the tunnel barrier result in the scatter of the R_nC data, which is consistent with our measurements. The scatter of the R_nC translates into the scatter in the more often used parameters, specific capacitance and R_nA. Those parameters are also dependent on the junction area and are thus affected by the uncertainty in the junction area estimation.

[1]P. Seidel, *Applied Superconductivity: Handbook on Devices and Applications* (Wiley-VCH, 2015).
[2]S. K. Tolpygo, V. Bolkhovsky, T. J. Weir, L. M. Johnson, M. A. Gouker, and W. D. Oliver, IEEE Trans. Appl. Supercond. **25**(3), 1101312 (2015).
[3]D. Nakada, K. K. Berggren, E. Macedo, V. Liberman, and T. P. Orlando, IEEE Trans. Appl. Supercond. **13**, 111 (2003).
[4]G. L. Kerber, L. A. Abelson, K. Edwards, and H. Roger, IEEE Trans. Appl. Supercond. **13**, 82 (2003).
[5]H. Numata and S. Tahara, IEICE Trans. Electron. **E84-C**, 2–8 (2001).
[6]A. W. Kleinsasser, F. M. Rammo, and M. Bhushan, Appl. Phys. Lett. **62**, 1017 (1993).
[7]M. G. Blamire, R. E. Somekh, Z. H. Barber, G. W. Morris, and J. E. Evetts, J. Appl. Phys. **64**, 6396 (1988).
[8]J. M. Rowell and W. L. Feldmann, Phys. Rev. **172**, 393 (1968).
[9]J. R. Schrieffer and J. W. Wilkins, Phys. Rev. Lett. **10**, 17 (1963).
[10]A. W. Kleinsasser, W. H. Mallison, R. E. Miller, and G. B. Arnold, IEEE Trans. Appl. Supercond. **5**, 2735 (1995).
[11]S. Oh, K. Cicak, R. McDermott, K. B. Cooper, K. D. Osborn, R. W. Simmonds, M. Steffen, J. M. Martinis, and D. P. Pappas, Supercond. Sci. Technol. **18**, 1396 (2005).
[12]K. M. Schep and G. E. W. Bauer, Phys. Rev. Lett. **78**, 3015 (1997).
[13]Y. Naveh, V. Patel, D. V. Averin, K. K. Likharev, and J. E. Lukens, Phys. Rev. Lett. **85**, 5404 (2000).
[14]V. Lacquaniti, M. Belogolovskii, C. Cassiago, N. De Leo, M. Fretto, and A. Sosso, New J. Phys. **14**, 023025 (2012).
[15]A. W. Kleinsasser, IEEE Trans. Appl. Supercond. **11**, 1043 (2001).
[16]W. H. Mallison, R. E. Miller, and A. W. Kleinsasser, IEEE Trans. Appl. Supercond. **5**, 2330 (1995).
[17]P. Y. Aghdam, H. Rashid, A. Pavolotsky, V. Desmaris, D. Meledin, and V. Belitsky, IEEE Trans. Terahertz Sci. Technol. **5**, 464 (2015).
[18]A. B. Pavolotsky, D. Dochev, and V. Belitsky, J. Appl. Phys. **109**, 024502 (2011).
[19]A. B. Ermakov, S. V. Shitov, A. M. Baryshev, V. P. Koshelets, and W. Luinge, IEEE Trans. Appl. Supercond. **11**, 840 (2001).
[20]H. Rashid, D. Meledin, V. Desmaris, A. Pavolotsky, and V. Belitsky, IEEE Trans. Terahertz Sci. Technol. **4**, 193 (2014).
[21]R. Dolata, H. Scherer, A. B. Zorin, and J. Niemeyer, J. Appl. Phys. **97**, 054501 (2005).
[22]T. Imamura and S. Hasuo, IEEE Trans. Appl. Supercond. **2**, 84 (1992).
[23]T. Imamura, Fujitsu Ltd., and S. Hasuo, IEEE Trans. Magn. **25**(2), 1131–1134 (1989).
[24]H. B. Palmer, Trans. Am. Inst. Electr. Eng. **56**, 363 (1937).
[25]J. Tucker and M. Feldman, Rev. Mod. Phys. **57**, 1055 (1985).
[26]H. Rashid, V. Desmaris, A. Pavolotsky, and V. Belitsky, in Proceedings of the 26th International Symposium on Space Terahertz Technology, Cambridge, MA, USA, 2015.

[27]P. Yadranjee Aghdam, *Characterisation of the Specific Capacitance of Superconducting Tunnel Junctions* (Chalmers University of Technology, 2015).

[28]M. Maezawa, M. Aoyagi, H. Nakagawa, I. Kurosawa, and S. Takada, Appl. Phys. Lett. **66**, 2134 (1995).

[29]H. S. J. van der Zant, R. A. M. Receveur, T. P. Orlando, and A. W. Kleinsasser, Appl. Phys. Lett. **65**, 2102 (1994).

[30]L. J. Zeng, S. Nik, T. Greibe, P. Krantz, C. M. Wilson, P. Delsing, and E. Olsson, J. Phys. D: Appl. Phys. **48**, 395308 (2015).

[31]T. Aref, A. Averin, S. van Dijken, A. Ferring, M. Koberidze, V. F. Maisi, H. Q. Nguyend, R. M. Nieminen, J. P. Pekola, and L. D. Yao, J. Appl. Phys. **116**, 073702 (2014).

[32]J. G. Simmons, J. Appl. Phys. **34**, 1793 (1963).

[33]J. C. Lau and R. V. Coleman, Phys. Rev. B **24**, 2985 (1981).

[34]J. B. Barner and S. T. Ruggiero, Phys. Rev. B **39**, 2060 (1989).

[35]J. Kadlec and K. H. Gundlach, Solid State Commun. **16**, 621 (1975).

[36]K. H. Gundlach and J. Hölzl, Surf. Sci. **27**, 125 (1971).